

Single particle properties of ^{16}O and ^{40}Ca

A. Fabrocini

INFN, Sezione di Pisa, I-56100 Pisa, Italy and

Department of Physics, University of Pisa, I-56100 Pisa, Italy

(November 16, 2018)

Abstract

We discuss some single particle properties of ^{16}O and ^{40}Ca using correlated basis function theory and Fermi hypernetted chain equations with central and tensor correlations. In particular, we concentrate on one body density matrix, momentum distribution, natural orbits and quasi hole states. The correlations are variationally generated by a realistic hamiltonian containing the Argonne v'_8 two-nucleon and Urbana IX three-nucleon interactions. The correlated momentum distributions show the well known enhancement at large momenta, with a relative importance of the different correlations (Jastrow and tensor) similar to that in nuclear matter. The natural orbits and their occupation numbers are obtained by diagonalization of the density matrix. The correlated first natural orbits occupations are depleted by more than 10%, whereas the first following ones are occupied by a few percent. The spectroscopic factors of the valence states are lowered by $\sim 8-12\%$ with respect to unity by central and tensor correlations, confirming that short range correlations alone are not able to explain the values extracted from $(e, e'p)$ experiments.

I. INTRODUCTION

The behavior of the single nucleon in the medium bears clear signatures of the nucleon–nucleon (NN) correlations induced by the strong nuclear interaction. The most celebrated one is the presence of high momentum components in the momentum distribution (MD), which may be explained only in terms of short range correlations (SRC) and cannot be justified by any independent particle model (IPM) [1,2]. In addition, both short– and long–range correlations (LRC) are now widely thought to be the origin of the large reduction of the spectroscopic strengths of the hole states [3].

In general, the investigation of SRC is one of the main topics in the physics of strongly interacting systems, from liquid Helium to nuclear matter. The translational invariance of homogeneous media has made possible a quantitative assesment of their importance in these contexts. However, the advances in realistic many–body theories have only recently allowed to address the same issue in inhomogeneous objects, as atomic nuclei, with a comparable accuracy. To this aim, correlated basis functions (CBF) theory has emerged as an effective tool to tackle the SRC problem in nuclear systems [4] when realistic hamiltonians are employed. When used in conjunction with the Fermi hypernetted chain (FHNC) integral equations [5,6], CBF has attained in ^{16}O and ^{40}Ca the same accuracy as in the best variational studies of nuclear matter [7,8].

In order to disentangle the SRC effects, one has to look at effects that go beyond any possible IPM description of the nucleus. SRC are mainly produced by the repulsive core of the NN interaction, whereas important intermediate and long range contributions (essentially of the tensor type) come from the exchange of one or more pions. This part of the nuclear interaction is the responsible of the nuclear binding [7]. Direct evidence of the SRC are not easy to experimentally single out and only in these last few years, thanks to the advances in the experimental techniques, there have been consistent efforts aimed to their identification. For instance, $(e, e'p)$ data in the quasi-elastic region need a large reduction of the IPM hole strength to be reproduced [9]. Moreover, charge density distributions obtained

by elastic electron scattering experiments are smaller than those predicted by the IPM [10] in the nuclear interior. These facts can be explained by assuming occupation probabilities of the single particle levels different from the IPM ones [11].

The basic quantity to investigate in order to verify the hypothesis of partial occupation probability is the one body density matrix (OBDM), $\rho(\mathbf{r}_1, \mathbf{r}_{1'})$, defined as:

$$\rho(\mathbf{r}_1, \mathbf{r}_{1'}) = \langle \Psi_0(A) | a^\dagger(\mathbf{r}_1) a(\mathbf{r}_{1'}) | \Psi_0(A) \rangle, \quad (1)$$

where $\Psi_0(A)$ is the ground state A-body wave function and $a^\dagger(a)(\mathbf{r}_1)$ is the creation (annihilation) operator of a nucleon at the position \mathbf{r}_1 . The Fourier transform of the OBDM gives the momentum distribution (MD), $n(k)$, sometimes used in plane wave impulse approximation to study inclusive and exclusive reactions. The natural orbits (NO) [12], with their occupation numbers (n_α), are defined as the basis where the OBDM is diagonal. In the IPM, the nuclear ground state is described by a Slater determinant of fully occupied single particle (SP) wave functions below the Fermi surface, α_F . So, the NO and the SP w.f. coincide, with $n_{\alpha \leq \alpha_F} = 1$ and $n_{\alpha > \alpha_F} = 0$. Deviations from this situation are a measure of the correlations, since they deplete the populated orbitals and allow higher NO to get $n_{\alpha > \alpha_F} \neq 0$.

Other important quantities are the quasihole (QH) wave functions, $\psi_h(\mathbf{r})$, defined as the overlaps between Ψ_0 and the hole states, Ψ_h , obtained by removing a nucleon from the position \mathbf{r} . From $(e, e'p)$ experiments it is possible to obtain an accurate determination of the QH overlap functions [13], whose normalizations give the spectroscopic factors, S_h . Typical values of S_h , as extracted from the experiments, are $S_h \sim 0.6 - 0.7$ [14], and the deviations from unity (their IPM value) come in account of various effects, from center of mass to correlation corrections.

In CBF theory the description of the correlations starts with an A-body correlated wave function

$$\Psi_0(1, 2 \dots A) = \mathcal{S} \left(\prod_{i < j} F_{ij} \right) \Phi_0(1, 2 \dots A), \quad (2)$$

corresponding to a symmetrized product of non commuting two-body correlation operators, F_{ij} , acting on the mean field wave function, $\Phi_0(1, 2 \dots A)$, given by a Slater determinant of single particle wave functions, $\phi_\alpha(i)$. A realistic choice of F_{ij} is:

$$F_{ij} = \sum_{p=1,6} f^p(r_{ij}) O_{ij}^p, \quad (3)$$

where

$$O_{ij}^{p=1,8} = [1, \boldsymbol{\sigma}_i \cdot \boldsymbol{\sigma}_j, S_{ij}, (\mathbf{L} \cdot \mathbf{S})_{ij}] \otimes [1, \boldsymbol{\tau}_i \cdot \boldsymbol{\tau}_j] \quad (4)$$

and $S_{ij} = (3 \hat{\mathbf{r}}_{ij} \cdot \boldsymbol{\sigma}_i \hat{\mathbf{r}}_{ij} \cdot \boldsymbol{\sigma}_j - \boldsymbol{\sigma}_i \cdot \boldsymbol{\sigma}_j)$ is the tensor operator.

The variational principle provides a natural recipe to determine the correlation functions, $f^p(r)$, and the single particle wave functions by minimizing the ground state energy. In our calculation we adopt a non relativistic nuclear hamiltonian of the form:

$$H = \frac{-\hbar^2}{2m} \sum_i \nabla_i^2 + \sum_{i<j} v_{ij} + \sum_{i<j<k} v_{ijk}, \quad (5)$$

where we have used the v'_8 reduction of the Argonne v_{18} [15] potential and the Urbana IX [16] three-nucleon interaction.

II. ONE BODY DENSITY MATRIX, MOMENTUM DISTRIBUTION AND NATURAL ORBITS

The one body density matrix (1) of doubly closed shell nuclei in (ls) coupling can be evaluated in FHNC [17], starting from

$$\rho(\mathbf{r}_1, \mathbf{r}_1') = \frac{A}{\mathcal{N}} \int d^3 r_2 \dots \int d^3 r_A \Psi_0^\dagger(1, 2, \dots A) \Psi_0(1', 2, \dots A), \quad (6)$$

where $\mathcal{N} = \int d^3 r_1 \dots \int d^3 r_A |\Psi_0|^2$ and A is the mass number. Once the OBDM is known, its diagonal part provides the one body density, $\rho_1(\mathbf{r}_1)$, and the momentum distribution may be computed by

$$n(k) = \frac{1}{A} \int d^3 r_1 \int d^3 r_1' \rho(\mathbf{r}_1, \mathbf{r}_1') e^{i\mathbf{k} \cdot (\mathbf{r}_1 - \mathbf{r}_1')}. \quad (7)$$

The independent particle model expression for the OBDM is well known and reads as:

$$\rho_{IPM}(\mathbf{r}_1, \mathbf{r}_{1'}) = \sum_{\alpha} \phi_{\alpha}^{\dagger}(1) \phi_{\alpha}(1'). \quad (8)$$

In the case of Jastrow correlated wave functions (when only the first component of the correlation (3) is retained), the density matrix may be expanded in powers of the *dynamical correlations*, $h(r) = [f^1(r)]^2 - 1$ and $\omega(r) = f^1(r) - 1$, and of the *statistical correlations*. The expansion generates cluster terms classified according to the number of particles and to the number of the correlation lines. The FHNC equations allow for summing cluster terms at all orders. Details of the finite systems FHNC theory may be found in Ref. [5,18]. The FHNC equations for the more general f_6 correlation of (3) were derived in Ref. [7,17] for the one and two body densities and for the OBDM.

The single particle wave functions needed to build the Slater determinant $\Phi_0(1, 2 \dots A)$ have been obtained by solving the single particle Schrödinger equation with a Woods–Saxon potential,

$$V_{WS}(r) = \frac{V_0}{1 + \exp[(r - R_0)/a_0]}, \quad (9)$$

whose parameters have been fixed to reproduce at best the nuclei empirical densities. This choice, while spoiling the binding energies by only a few percent with respect to a full minimization, provides an accurate description of the nuclear densities [8].

The correlated momentum distributions computed within the CBF scheme are shown in Fig.1. The MDs of ^{16}O (continuous line) and of ^{40}Ca (dashed line) are compared with that of nuclear matter with Jastrow (thin solid line) and full (dash–dotted line) correlations. The IPM momentum distributions are given by squares (^{16}O) and stars (^{40}Ca). We stress that the differences between the Jastrow and the f_6 correlations are similar in the infinite and finite systems and that the three cases show an analogous behavior in large momentum region, that is dominated by the short range structure (and the NN correlations) of the nuclear wave function. The effect is, to a large extent, independent on the nucleus. The tensor correlations enhance the tails of the MDs by a factor 2–3 with respect to the Jastrow

case, slightly smaller than that found in Ref. [19] (~ 4). The difference may be understood in terms of the stronger tensor force of the Argonne v_{14} potential adopted in that reference, and of the presence of spin-orbit correlations, omitted in our calculation.

Another piece of information that can be extracted from the OBDM are the natural orbits and their occupation numbers. The NO are obtained by diagonalizing the OBDM:

$$\rho_1(\mathbf{r}_1, \mathbf{r}_{1'}) = \sum_{\alpha} n_{\alpha} \phi_{\alpha}^{NO}(\mathbf{r}_1)^{\dagger} \phi_{\alpha}^{NO}(\mathbf{r}_{1'}). \quad (10)$$

For spherical nuclei in (ls) single particle coupling, saturated in both spin and isospin, this expression can be recast as:

$$\rho_l(\mathbf{r}_1, \mathbf{r}_{1'}) = \nu \sum_l \frac{2l+1}{4\pi} P_l(\cos \theta_{11'}) \rho_l(r_1, r_{1'}), \quad (11)$$

where $P_l(x)$ are the Legendre polynomials, $\theta_{11'}$ is the angle between \mathbf{r}_1 and $\mathbf{r}_{1'}$ and $\nu=4$ is the nucleon degeneracy. Exploiting again the spherical symmetry, one obtains

$$\rho_l(r_1, r_{1'}) = \nu \sum_n n_{nl} \phi_{nl}^{NO}(r_1) \phi_{nl}^{NO}(r_{1'}). \quad (12)$$

The first three NO of ^{16}O and ^{40}Ca are shown in Figs. 2. The NO occupation numbers for Jastrow and f_6 correlations are given in Table I. The effect of the correlations on the shell model orbitals are mainly visible in the short range part of the $1s$ state, making this NO more localized than its IPM counterpart. The shape of the other IPM states is barely influenced. The occupation of the NO corresponding to the shell model ones is depleted by as much as 22% (the $2s$ state in ^{40}Ca). In contrast, the mean field unoccupied states become sizeably populated. The two effects are largely due to the tensor correlations.

The Green function (GF) approach of Ref. [20] found the ^{16}O $n=1$ NO more populated than the CBF ones for the occupied shell model states ($l=0, 1$), and, consequently, lower occupations for all the remaining orbitals ($n_{1s}^{GF}=.921$, $n_{1p}^{GF}=.941$ and $n_{1d}^{GF}=.017$. The $1p$ ($1d$) occupation numbers are the average of the $1p_{1/2}$ and $1p_{3/2}$ ($1d_{3/2}$ and $1d_{5/2}$) orbitals of the reference). These discrepancies are probably due to the different potentials adopted, rather than to the methodologies. In fact, in the GF calculation the one-boson-exchange Bonn

B potential [21] was used. The A8'+UIX model induces stronger correlations, so giving a larger depletion of the lowest NO. A similar effect was found in ^3He atomic drops [22], where the strong repulsive interaction between the ^3He atoms depletes the shell model occupations by 15–46 %.

III. SINGLE PARTICLE OVERLAPS

In a fixed center reference frame, the overlap between the A-body ground-state and the (A-1)-body hole state of the residual system, ψ_h , is given by

$$\psi_h(x) = \sqrt{A} \frac{\langle \Psi_h(A-1) | \delta(x - x_A) | \Psi_0(A) \rangle}{\langle \Psi_h(A-1) | \Psi_h(A-1) \rangle^{1/2} \langle \Psi_0(A) | \Psi_0(A) \rangle^{1/2}}. \quad (13)$$

In CBF theory $\Psi_h(1, 2 \dots A-1)$ is built by substituting $\Phi_0(1, 2 \dots A)$ in (2) with the Slater determinant obtained by removing a nucleon in the state h , $\Phi_h(1, 2 \dots A-1)$. In doubly closed shell nuclei in the ls coupling scheme the radial dependence of the overlap function can be singled out, as

$$\psi_h(x) = \psi_h(r) Y_{lm}(\hat{r}) \chi_{\sigma\tau}, \quad (14)$$

where $\chi_{\sigma\tau}$ is the spin-isospin single particle wave function. In the IPM, the overlaps are simply the shell model functions and $\psi_h^{IPM}(r) = R_{h=nl}(r)$, where $R_h(r_i)$ is the radial part of $\phi_\alpha(i)$.

In order to develop a cluster expansion for $\psi_h(r)$, its expression is rearranged as:

$$\psi_h(r) = \mathcal{X}_h(r) \mathcal{N}_h^{1/2}, \quad (15)$$

where

$$\mathcal{X}_h(r) = \sqrt{A} \frac{\langle \Psi_h(A-1) | Y_{lm}(\hat{r}) \chi_{\sigma\tau} \delta(\mathbf{r} - \mathbf{r}_A) | \Psi_0(A) \rangle}{\langle \Psi_h(A-1) | \Psi_h(A-1) \rangle}, \quad (16)$$

and

$$\mathcal{N}_h = \frac{\langle \Psi_h(A-1) | \Psi_h(A-1) \rangle}{\langle \Psi_0(A) | \Psi_0(A) \rangle}. \quad (17)$$

Cluster expansions and FHNC-like equations are then used to compute \mathcal{X}_h and \mathcal{N}_h [17], along the lines given in Ref. [23] to evaluate the overlap matrix elements in the CBF study of the nuclear matter spectral function.

Finally, the spectroscopic factor, S_h , is given by the quasihole normalization,

$$S_h = \int r^2 dr \psi_h^2(r). \quad (18)$$

The independent particle model gives $S_h^{IPM} = 1$. Center of mass (*cm*) corrections are a first source of correction. In fact, in the harmonic oscillator model they enhance S_h for the valence hole states (those having the largest oscillator quantum number, N_v) by the $[A/(A-1)]^{N_v}$ factor [24]. So, the *cm*-corrected $1p$ -shell spectroscopic factor of ^{16}O is $S_{1p,cm}^{HO} = 16/15 \sim 1.07$, while the average between the $2s$ and $1d$ states in ^{40}Ca is $S_{2s/1d,cm}^{HO} = (40/39)^2 \sim 1.05$. Similar results are found with the more realistic Woods-Saxon orbitals [25].

The correlated spectroscopic factors (without *cm* corrections) in ^{16}O and ^{40}Ca are shown in Table II for f_6 and Jastrow correlations. Jastrow correlations marginally reduce S_h (at most 3%). Central spin-isospin correlations also provide a few percent depletion in the valence states, whereas the tensor correlations (f_6) give most of the reduction. For instance, they lower S_{1p} in ^{16}O to 0.90 and S_{2s} and S_{1d} in ^{40}Ca to 0.86 and 0.87, respectively. The $1p$ CBF ^{16}O result fully agrees with the variational Monte Carlo estimate of Ref. [25]. The operatorial correlations largely influence the low lying states, whose spectroscopic factors are drastically reduced by both central and tensor components: S_{1s} in ^{16}O is 0.70, S_{1p} and S_{1s} in ^{40}Ca are 0.58 and 0.55, respectively.

The latest experimental values of S_p from the $^{16}\text{O}(e, e'p)^{15}\text{N}$ reaction [26] are $S_{p_{1/2}}=0.61$ for the $1/2^-$ ground state in ^{15}N and $S_{p_{3/2}}(6.32)=0.53$ for the lowest $3/2^-$ state at 6.32 MeV. This state exhibits 87% of the total $S_{p_{3/2}}$ strength, that is fragmented over three states at 6.32, 9.93 and 10.70 MeV. The total $S_{p_{3/2}}$ may be estimated to be $S_{p_{3/2}}=0.53/0.87=0.61$ [25]. In the $^{40}\text{Ca}(e, e'p)^{39}\text{K}$ reaction [14] the transition to the $1d_{3/2}$ ground state gives $S_{d_{3/2}} \sim 0.61 \pm 0.07$. We recall that the CBF values are $S_p = 0.90$ in ^{16}O and $S_d = 0.87$ in ^{40}Ca .

The squared overlap functions are shown in Fig.3 for the Jastrow and f_6 correlations,

and are compared with the IPM ones. Jastrow components have little effect on the overlaps, while the spin–isospin correlations are the main responsible for the quenching of the IPM overlaps and of the spectroscopics factors.

The IPM results obtained by a Woods–Saxon potential fitting the $^{16}\text{O}(e, e'p)^{15}\text{N}$ cross section to the 6.32 MeV state with $S_{p_{3/2}}(6.32)=0.53$ are shown in the $|\psi_{1p}|^2-^{16}\text{O}$ panel as stars. We have rescaled $|\psi_{1p, FHNC}|^2$ by the factor $0.53/0.90$ and the result is in nice agreement with the empirical estimate.

IV. CONCLUSIONS

In this contribution we have presented some results obtained within the correlated basis functions theory and concerning the properties of the single nucleon in the nuclear medium. More specifically, we have discussed the behavior of the one-body density matrix and some related quantities, as the momentum distributions and the natural orbits, in ^{16}O and ^{40}Ca using the Fermi hypernetted chain resummation technique. In addition, we have addressed the evaluation of the overlap functions and of the spectroscopic factors within the same approach. The relevance of the short range correlations, both of central and tensor type, has been stressed. The results presented here have been obtained using the Argonne v'_8 two–nucleon potential plus the Urbana IX three–nucleon interaction, together with a set of single particle wave functions fixed to reproduce at best the empirical charge distributions of the two nuclei.

The high momentum tail of the momentum distribution is largely dominated by correlations, and tensor components enhance the tail by a factor 3–4 with respect to the central ones. The tensor correlation is also important for the occupation of the natural orbits. In fact, the reduction of the occupation of the levels below the Fermi surface and, conversely, the enhancement above is amplified by the tensor terms. As far as the correlated overlap functions are concerned, they are close to the single particle wave functions if central correlations are used, whereas their shapes are strongly modified by the tensor correlations. The

overall spectroscopic factors are depleted by 10-15%, for the valence levels and 30-45% for the deeply lying ones.

In spite of this reduction, the FHNC approach in ^{16}O does not reproduce the empirical $S_{p_{3/2}}$ spectroscopic factor extracted from $(e, e'p)$ reactions. A similar situation was met in Ref. [27] for nuclear matter, where the variational calculation of the one-hole strength, $Z(e)$, around the Fermi level provided $Z_v(e \sim e_F) \sim 0.88$, mostly due to tensor correlations. Second order perturbative corrections in a correlated basis, including two-hole one-particle, $(2h - 1p)$, correlated states, brought the strength to $Z_{CBF}(e \sim e_F) \sim 0.70$. This decrease explains almost half of the discrepancy with the empirical ^{208}Pb spectroscopic factor, $Z(^{208}\text{Pb}) \sim 0.5 - 0.6$. The missing strength can be attributed to the coupling of the single particle waves to the collective low-lying surface vibrations, not reproducible in infinite nuclear matter. It is expected that the inclusion of correlated $2h - 1p$ corrections in the finite nuclei calculations can similarly take into account the coupling with surface vibrations.

ACKNOWLEDGMENTS

The results presented in this contribution have been obtained in collaboration with Giampaolo Co'. This work has been partially supported by MURST through the *Progetto di Ricerca di Interesse Nazionale: Fisica teorica del nucleo atomico e dei sistemi a multicorpi*.

REFERENCES

- [1] J. G. Zabolitzky and W. Ey, Phys. Lett. B **76**, 527 (1978); O. Bohigas and S. Stringari, Phys. Lett. B **95**, 9 (1980); M. Dal Rì, S. Stringari and O. Bohigas, Nucl. Phys. A **376**, 81 (1982); F. Dellagiacomma, G. Orlandini and M. Traini, Nucl. Phys. A **393**, 95 (1983); M. Jaminon, C. Mahaux and H. Ngô, Nucl. Phys. A **473**, 509 (1987).
- [2] A. N. Antonov, P. E. Hodgson and I. Zh. Petkov *Nucleon momentum and density distributions* (Clarendon Press, Oxford, 1988).
- [3] G. van der Steenhoven and P. K. A. de Witt Huberts, in *Modern Topics in Electron Scattering*, edited by B. Frois and I. Sick (World Scientific, Singapore, 1991), p.510.
- [4] R. B. Wiringa, V. Ficks, and A. Fabrocini, Phys. Rev. C **38**, 1010 (1988).
- [5] G. Co', A. Fabrocini, S. Fantoni, and I. E. Lagaris, Nucl. Phys. A **549**, 439 (1992).
- [6] F. Arias de Saavedra, G. Co', A. Fabrocini, and S. Fantoni, Nucl. Phys. A **605**, 359 (1996).
- [7] A. Fabrocini, F. Arias de Saavedra, G. Co', and P. Folgarait, Phys. Rev. C **57**, 1668 (1998).
- [8] A. Fabrocini, F. Arias de Saavedra, and G. Co', Phys. Rev. C **61**, 044302 (2000).
- [9] P. K. A. de Witt Huberts, J. Phys. G **16**, 507 (1990).
- [10] J.M. Cavedon *et al.*, Phys. Rev. Lett. **49**, 978 (1982).
- [11] C. Papanicolas, in *Nuclear Structure at high spin, excitation and momentum transfer*, H. Nann ed., (American Institute of Physics, New York 1986), p. 110.
- [12] C. Mahaux and R. Sartor, Adv. Nucl. Phys. **20**, 1 (1991).
- [13] J. J. Kelly, Adv. Nucl. Phys. **23**, 75 (1996).
- [14] L. Lapikás, Nucl. Phys. A **553**, 297c (1993).

- [15] R. B. Wiringa, V. G. J. Stoks, and R. Schiavilla, Phys. Rev. C **51**, 38 (1995).
- [16] B. S. Pudliner, V. R. Pandharipande, J. Carlson, S. C. Pieper, and R. B. Wiringa, Phys. Rev. C **56**, 1720 (1997).
- [17] A. Fabrocini, and G. Co', Phys. Rev. C **63**, 0443109 (2001).
- [18] G. Co', A. Fabrocini, and S. Fantoni, Nucl. Phys. A **568**, 73 (1994).
- [19] S. C. Pieper, R. B. Wiringa, and V. R. Pandharipande, Phys. Rev. C **46**, 1741 (1992).
- [20] A. Polls, H. Müther, and W. H. Dickhoff, Nucl. Phys. A **594**, 117 (1995).
- [21] R. Machleidt, Adv. Nucl. Phys. **19**, 1 (1989).
- [22] D. S. Lewart, V. R. Pandharipande, and S. C. Pieper, Phys. Rev. B **37**, 4950 (1988).
- [23] O. Benhar, A. Fabrocini, and S. Fantoni, Nucl. Phys. A **505**, 267 (1989).
- [24] A. E. L. Dieperink, and T. de Forest, Phys. Rev. C **10**, 543 (1974).
- [25] D. Van Neck, M. Waroquier, A. E. L. Dieperink, S. C. Pieper, and V. R. Pandharipande, Phys. Rev. C **57**, 2308 (1998).
- [26] M. Leuscher *et al.*, Phys. Rev. C **49**, 955 (1994).
- [27] O. Benhar, A. Fabrocini and S. Fantoni, Phys. Rev. C **41**, R24 (1990).

TABLES

TABLE I. Occupation numbers of the nl -th natural orbits for ^{16}O and ^{40}Ca in CBF, with the f_6 and Jastrow correlation models.

nl	$n_{nl}(f_6; ^{16}\text{O})$	$n_{nl}(\text{J}; ^{16}\text{O})$	$n_{nl}(f_6; ^{40}\text{Ca})$	$n_{nl}(\text{J}; ^{40}\text{Ca})$
$1s$	0.858	0.960	0.864	0.952
$2s$	0.019	0.005	0.780	0.962
$3s$	0.010	0.002	0.052	0.002
$4s$	0.005	0.001	0.013	0.001
$1p$	0.919	0.980	0.841	0.949
$2p$	0.021	0.004	0.024	0.009
$3p$	0.011	0.003	0.016	0.006
$1d$	0.025	0.006	0.956	0.983
$2d$	0.011	0.003	0.030	0.007
$3d$	0.006	0.001	0.019	0.006

TABLE II. CBF spectroscopic factors for ^{16}O and ^{40}Ca , with Jastrow (J) and f_6 correlations.

	corr.	$1s$	$1p$	$1d$	$2s$
^{16}O	J	0.98	0.98		
	f_6	0.70	0.90		
^{40}Ca	J	0.98	0.99	0.97	0.98
	f_6	0.55	0.58	0.87	0.86

FIGURES

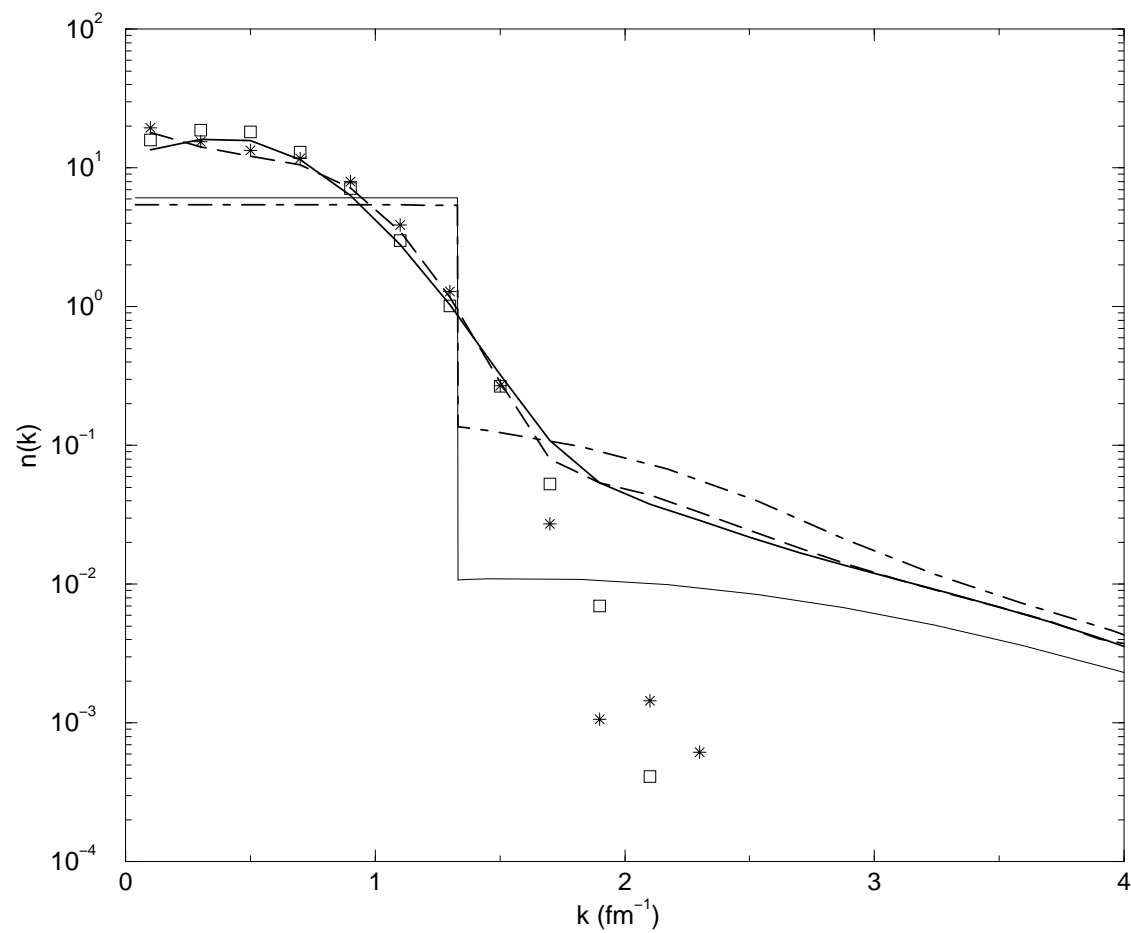


FIG. 1. Correlated momentum distributions in ^{16}O , ^{40}Ca and nuclear matter (NM). See text.

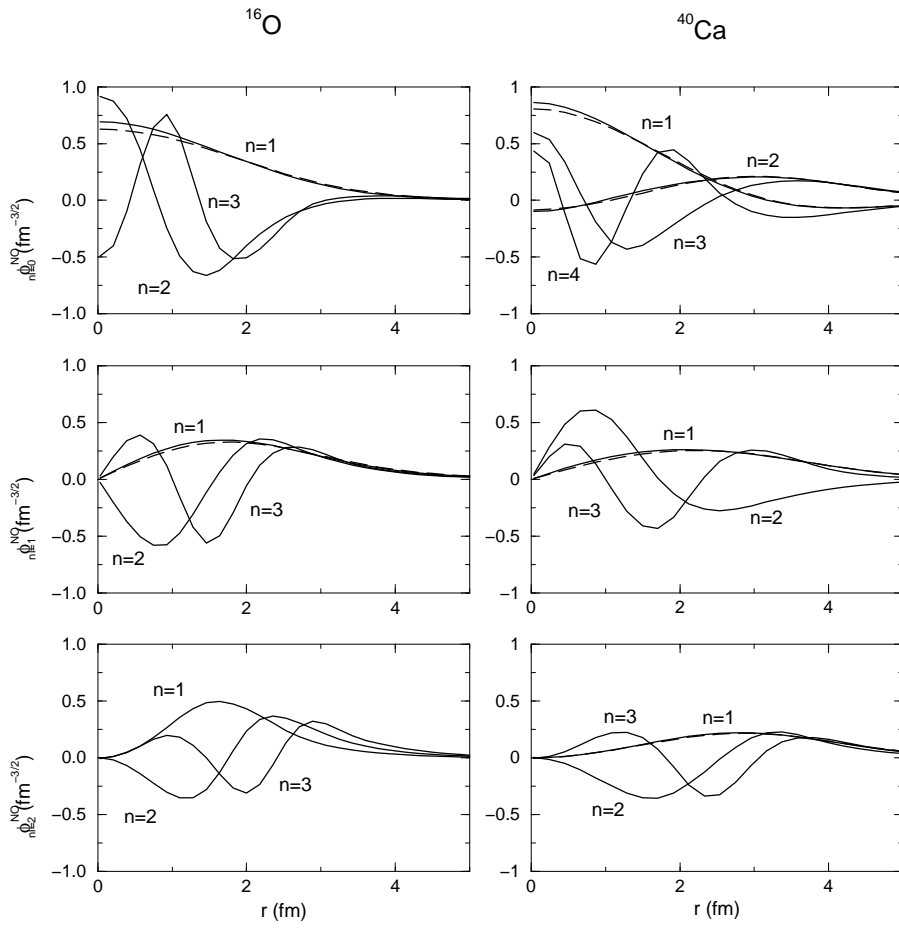


FIG. 2. Natural orbits of ^{16}O and ^{40}Ca . Solid lines: f_6 model; dashed: IPM.

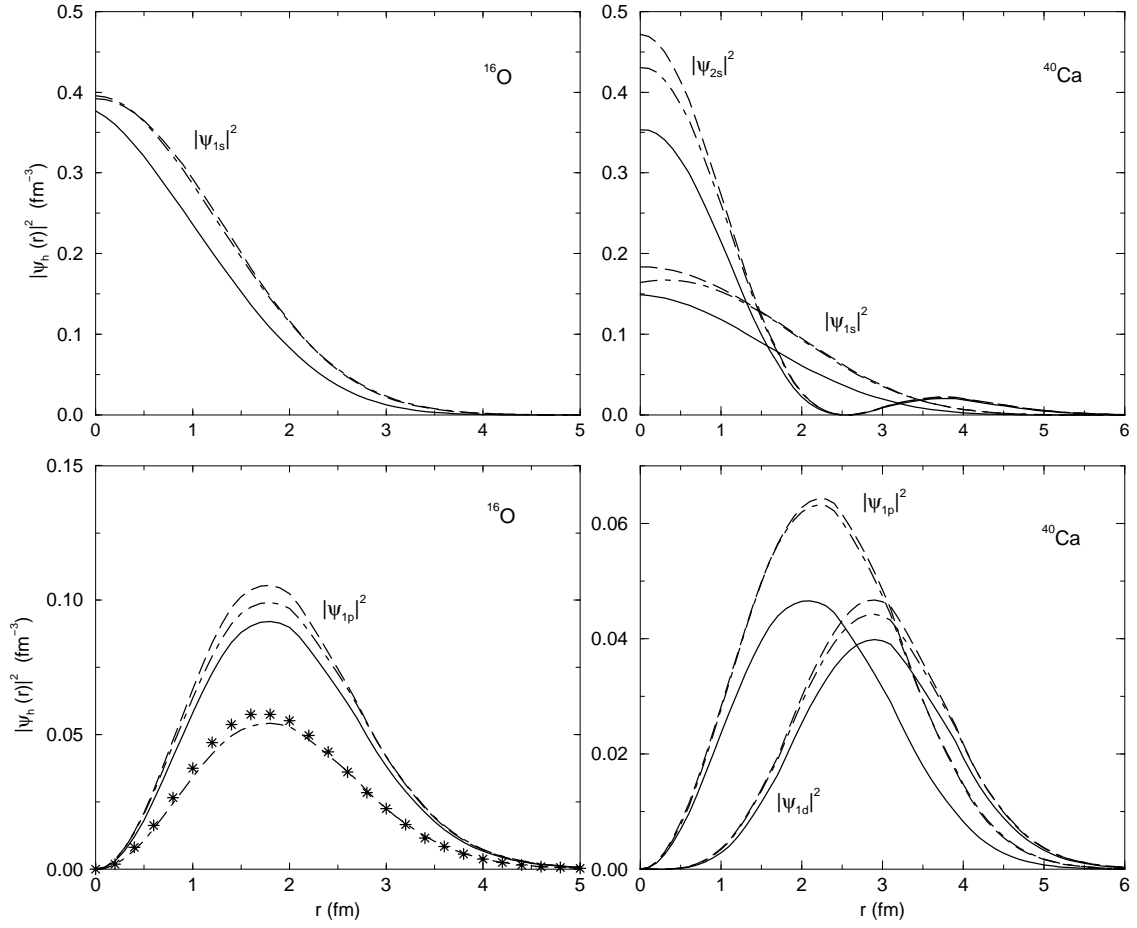


FIG. 3. Squared quasihole wave functions. Solid lines: f_6 model; dot-dashed: Jastrow; dashed: IPM. The $1p$ panel of ^{16}O shows also the empirical overlap (stars) and the f_6 one, rescaled as explained in the text (lower dot-dashed line)